

# Decentralized passivity-based control for cooperative power modules in the DC Microgrid System

Jesús Linares Flores \* Fernando A. Navarro Martínez \*\*  
Arturo Hernández Méndez \*\*\* José Antonio Juárez Abad \*\*\*\*  
Juan J. Montesinos †

\* *Universidad Tecnológica de la Mixteca, Oaxaca, 69000 México*  
(e-mail: [jlinares@mixteco.utm.mx](mailto:jlinares@mixteco.utm.mx))  
\*\* (e-mail: [fernando305.fm@gs.utm.mx](mailto:fernando305.fm@gs.utm.mx))  
\*\*\* (e-mail: [arturo@mixteco.utm.mx](mailto:arturo@mixteco.utm.mx))  
\*\*\*\* (e-mail: [abad@mixteco.utm.mx](mailto:abad@mixteco.utm.mx))  
† (e-mail: [jmontesinos@mixteco.utm.mx](mailto:jmontesinos@mixteco.utm.mx))

---

**Abstract:** This article deals with the decentralized passivity-based controller (PBC) design for the power modules DC/DC and AC/DC connected to a DC microgrid. The DC power modules use buck and boost topologies, while the AC/DC rectifier employs the boost topology. Linear extended state observers are used to estimate the load current demand by the DC microgrid. Thus, the power modules get equitable contribution and synchronization. The PSIM simulation results show the effectiveness and robustness of the decentralized passivity-based controllers of the power modules for the DC microgrid system.

*Keywords:* DC Microgrid, Cooperative Power Modules, Decentralized Passivity-based Control.

---

## 1. INTRODUCTION

The constant search for energy efficiency has driven innovations, such as microgrids Modu et al. (2023), which stand out in a sustainable generation. Amid the accelerated transition to renewable energy, microgrids are emerging as a technology that integrates diverse sources for more efficient and sustainable generation Al-Ismaïl (2021); Espina et al. (2020). Advances in power electronics enable decentralized controllers for microgrid power modules. Renewable energy sources, such as photovoltaic panels connected to a battery or a load, are built through the microgrid concept. They implement power circuits to raise the voltage (buck converter), obtaining electrical power to support human development, as mentioned in the literature Anand and Fernandes (2013); Bai et al. (2020); El-Shahat and Sumaiya (2019). On the other hand, Loranca-Coutiño et al. (2022) mentions that modeling is the most common control practice, where we typically assume that all the elements of the network and their models are known a priori. Unfortunately, this is not the general case in practice since the DC microgrid is subject to continuous changes due to its modular nature. Additionally, they say this issue becomes even more relevant when the converter-load combinations are not predicted during the control design stage, this can cause instability Feng et al. (2002); Liu et al. (2003). Another major challenge from a model-

based perspective is that many active and passive devices involve many state variables and equations.

Thus, this motivates the proposal of a passivity-based controller that adapts to continuous changes due to the modular nature of the DC microgrid. This proposal is based on an Extended State Observer to estimate parameters, state variables, and internal and external perturbations to reduce the effects of the converter-load combinations and, in this way, ensure the stability of the DC microgrid system. The ease of the design of the passivity-based controllers and extended state observers in each DC generation power module makes it possible to solve many problems subject to a DC microgrid system.

### 1.1 Contributions

The main contribution is using three different topologies for DC power generation in a DC microgrid system, Fig. 1. The respective passivity-based control laws and extended state observers (ESOs) achieve local stability in the closed loop in each power converter. Employing ESOs, the passivity-based controllers make an equitable power contribution and synchronize the interconnection node of the DC microgrid. To evaluate the effectiveness and robustness of the closed-loop system using the PSIM simulation program.

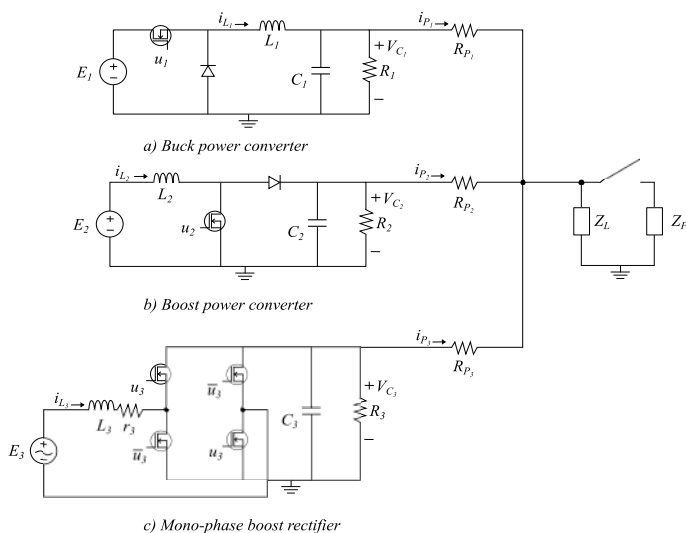


Fig. 1. Three power modules of the DC Microgrid System.

## 2. DESCENTRALIZED PASSIVITY-BASED CONTROL DESIGNS

This section deals with the design of DC power generation modules. The first and second power modules are DC/DC buck converters and DC/DC boost converters, while the third power module is a mono-phase rectifier boost type. We use their corresponding average models to design the passivity-based controllers of the DC power generation modules. These controllers adapt the output currents according to the demand at the interconnection node of the DC microgrid.

### 2.1 Modeling and ESO-PBC for the DC/DC Buck power converter

From the circuit in Fig. 1 (a), we obtain the following average model of the buck power converter.

$$L_1 \frac{di_{L_1}}{dt} = -v_{C_1} + E_1 u_1 \quad (1)$$

$$C_1 \frac{dv_{C_1}}{dt} = i_{L_1} - \left( \frac{1}{R_1} \right) v_{C_1} - i_{p_1} \quad (2)$$

From (1)-(2), we write to the buck power converter system in its passive form as follows:

$$A\dot{x} = (J - R)x + Bu_1 + \eta \quad (3)$$

where,

$$\begin{aligned} x &= (i_{L_1} \ v_{C_1})^T \in \mathbb{R}^2; \ u_1 \in \mathbb{R}; \ B = (E_1 \ 0)^T \\ A &= \begin{pmatrix} L_1 & 0 \\ 0 & C_1 \end{pmatrix}; \ J = \begin{pmatrix} 0 & -1 \\ 1 & 0 \end{pmatrix}; \\ R &= \begin{pmatrix} 0 & 0 \\ 0 & \frac{1}{R_1} \end{pmatrix}; \ \eta = (0 \ -i_{p_1})^T; \end{aligned} \quad (4)$$

Making a true copy from (3), we have the following dynamic desired system,

$$A\dot{x}^* = (J - R)x^* + Bu_1^* + \eta^* \quad (5)$$

where the desired input vector of perturbation adapts the estimated output current given by  $\widehat{i_{p_1}}$ , thus we have to  $\eta^*$  as follows

$$\eta^* = \begin{pmatrix} 0 \\ -\widehat{i_{p_1}} \end{pmatrix}$$

The error dynamics is obtained from (3) and (5), where we define to as  $e = x - x^*$ ,  $e_{u_1} = u_1 - u_1^*$ , and  $e_\eta = \eta - \eta^*$ . Therefore, we have

$$A\dot{e} = (J - R)e + Be_{u_1} + e_\eta \quad (6)$$

The Lyapunov candidate function is defined as follows

$$V(e) = \frac{1}{2} e^T A e > 0 \quad (7)$$

Its time derivative is given by

$$\dot{V}(e) = e^T A \dot{e} \quad (8)$$

Substituting (6) in (8), yields the following

$$\begin{aligned} \dot{V}(e) &= e^T ((J - R)e + Be_{u_1} + e_\eta) \\ &= -e^T R e + e^T B e_{u_1} + e^T e_\eta \end{aligned} \quad (9)$$

We choose the following error input control law

$$\begin{aligned} e_{u_1} &= -\gamma B^T e \\ \gamma &> 0 \end{aligned} \quad (10)$$

We incorporate (10) in (9), where we consider that error of the perturbation is radially enclosure. Thus, we have

$$\begin{aligned} \dot{V}(e) &= -e^T R e - e^T \underbrace{\gamma B B^T}_{:=R_d} e + e^T e_\eta \\ &= -e^T \underbrace{(R + R_d)}_{:=\tilde{R}} e + e^T e_\eta \\ &= -e^T \tilde{R} e + e^T e_\eta \end{aligned} \quad (11)$$

Notice that  $\tilde{R}$  is a diagonal matrix positive definite, with its diagonal elements are greater than one, then it can be shown that  $e_\eta = 0$  implies that  $e = 0$  is a globally exponentially stable equilibrium since

$$\dot{V}(e) = -e^T \tilde{R} e < 0 \quad (12)$$

On the other hand, if the error of perturbation current estimation  $e_\eta \neq 0$ , then (11) is given as follow:

$$\dot{V}(e) = -(1 - \phi)e^T \tilde{R} e - \phi e^T \tilde{R} e + e^T e_\eta$$

with  $\phi > 0$  being a positive constant which belongs to set  $(0, 1)$ . Thus, we obtain

$$\dot{V}(e) = -(1 - \phi)e^T \tilde{R} e < 0 \quad (13)$$

whenever (using Young's inequality), we write

$$e^T e_\eta \leq k |e^T|^2 + \frac{1}{4k} |e_\eta|^2 \leq \phi e^T \tilde{R} e$$

where  $k > 0$ . On the other hand, the linear extended state observer (LESO) design is built from (2). For this we make the following considering,  $y_1 = \hat{v}_{C_1}$ ,  $y = v_{C_1}$ , and  $\eta_1 = \widehat{i_{p_1}}$ . Therefore, we have

$$C_1 \frac{dy_1}{dt} = \underbrace{i_{L_1}}_{:=u_{obs}} - \left(\frac{1}{R_1}\right) y_1 + \eta_1 + \lambda_1 (y - y_1)$$

$$\frac{d\eta_1}{dt} = \lambda_0 (y - y_1) \quad (14)$$

From (2) and (14), we obtain the error observation dynamics,

$$\ddot{e}_{obs} + \left(\frac{1}{R_1} + \lambda_1\right) \dot{e}_{obs} + \lambda_0 e_{obs} = -\frac{d}{dt} i_{p1} \quad (15)$$

The selection of observer gains

$$\lambda_1 = 2\zeta\omega_n - \left(\frac{1}{R_1}\right); \lambda_0 = \omega_n^2$$

$$\omega_n \geq \frac{1}{RC}, \zeta = 0.707 \quad (16)$$

with these gains the observation error  $e_{obs}$  converges asymptotically to near zero when  $t \rightarrow \infty$ , which produces that  $e_\eta = i_{p1} - \widehat{i}_{p1}$  is radially enclosure and converges asymptotically to near zero. From (10), we obtain the passivity-based controller

$$u_1 = \bar{u}_1 - \gamma_1 (i_{L_1} - \bar{i}_{L_1}) \quad (17)$$

The constant desired references of the passivity-based controller (17) are

$$\bar{u}_1 = \frac{V_{d1}}{E_1}, \bar{i}_{L_1} = \frac{V_{d1}}{R_1} + \eta_1 \quad (18)$$

where  $V_{d1}$  is the constant-desired reference of the output voltage of the buck power converter, and  $E_1$  is the power source supply.

Notice that the estimated variable of the DC interconnection node output current,  $\eta_1$ , is adapted to the inductor current desired reference of the buck converter to obtain an equitable active power contribution and synchronization with the rest of the DC power modules.

## 2.2 Modelling and ESO-PBC for the DC/DC Boost power converter

The average model of the boost power converter is shown in Fig. 1 (b), which is given by

$$L_2 \frac{di_{L_2}}{dt} = -v_{C_2} u_2 + E_2 \quad (19)$$

$$C_2 \frac{dv_{C_2}}{dt} = i_{L_2} u_2 - \left(\frac{1}{R_2}\right) v_{C_2} - i_{p2} \quad (20)$$

From (19) and (20), we write the buck-power converter in its passive form

$$A\dot{x} = J(u_2)x - Rx + \eta \quad (21)$$

where,

$$x = (i_{L_2} \ v_{C_2})^T \in R^2; u_2 \in R;$$

$$A = \begin{pmatrix} L_2 & 0 \\ 0 & C_2 \end{pmatrix}; J(u_2) = \begin{pmatrix} 0 & -u_2 \\ u_2 & 0 \end{pmatrix}; \quad (22)$$

$$R = \begin{pmatrix} 0 & 0 \\ 0 & \frac{1}{R_2} \end{pmatrix}; \eta = (E_2 \ -i_{p2})^T;$$

Making a true copy from (21), we have the following dynamic desired system:

$$A\dot{x}^* = J(u_2^*)x^* - Rx^* + \eta^* \quad (23)$$

where the desired input vector of perturbation adapts the estimated output current given by  $\widehat{i}_{p2}$ , thus we have to  $\eta^*$

$$\eta^* = \begin{pmatrix} E_2 \\ -\widehat{i}_{p2} \end{pmatrix}$$

The error dynamics is obtained from (3) and (5), where we define to as  $e = x - x^*$ ,  $e_{u2} = u_2 - u_2^*$ , and  $e_\eta = \eta - \eta^*$ . Therefore, we have

$$A\dot{e} = J(u_2)e + (J(u_2) - J(u_2^*))x^* - Re + e_\eta \quad (24)$$

Making an approximate linearization with respect to  $u_2$  for  $J(u_2)$ , we have the following

$$J(u_2) - J(u_2^*) = \frac{\partial J(u_2)}{\partial u_2} e_{u2} \quad (25)$$

The Lyapunov candidate function is defined as follows

$$V(e) = \frac{1}{2} e^T A e > 0 \quad (26)$$

Its time derivative is given by

$$\dot{V}(e) = e^T A \dot{e} \quad (27)$$

Substituting (25) in (27), yields the following

$$\dot{V}(e) = e^T J(u_2)e + e^T (J(u_2) - J(u_2^*))x^* - Re + e_\eta \quad (28)$$

We choose the following error input control law

$$e_{u2} = -\gamma \left( \frac{\partial J(u_2)}{\partial u_2} x^* \right)^T e$$

$$\gamma > 0 \quad (29)$$

We incorporate (29) in (28), where we consider that error of the perturbation is radially enclosure thus, we have

$$\dot{V}(e) = -e^T R e - e^T \underbrace{\gamma \frac{\partial J(u_2)}{\partial u_2} x^* \left( \frac{\partial J(u_2)}{\partial u_2} x^* \right)^T}_{:=R_d} e + e^T e_\eta$$

$$= -e^T \underbrace{(R + R_d)}_{:=\tilde{R}} e + e^T e_\eta$$

$$= -e^T \tilde{R} e + e^T e_\eta \quad (30)$$

Notice that  $\tilde{R}$  is a diagonal matrix positive definite, with its diagonal elements are greater than one, then it can be shown that  $e_\eta = 0$  implies that  $e = 0$  is a globally exponentially stable equilibrium since

$$\dot{V}(e) = -e^T \tilde{R} e < 0 \quad (31)$$

On the other hand, if the error of perturbation current estimation  $e_\eta \neq 0$ , then (30) is given as follow:

$$\dot{V}(e) = -(1 - \phi)e^T \tilde{R} e - \phi e^T \tilde{R} e + e^T e_\eta$$

with  $\phi > 0$  being a positive constant which belongs to set  $(0, 1)$ . Thus, we obtain

$$\dot{V}(e) = -(1 - \phi)e^T \tilde{R}e < 0 \quad (32)$$

whenever (using the Young's inequality), we write

$$e^T e_\eta \leq k |e^T|^2 + \frac{1}{4k} |e_\eta|^2 \leq \phi e^T \tilde{R}e$$

The passivity control law for the boost power converter (29) Linares-Flores et al. (2023), is described by

$$u_2 = \bar{u}_2 + \gamma_2 V_{d_2} (i_{L_2} - \bar{i}_{L_2}) - \gamma_2 \bar{i}_{L_2} (v_{C_2} - V_{d_2}) \quad (33)$$

On the other hand, the nonlinear average model (19)-(20) is exact linearization. Thus, we design a reduced extended state observer, considering only the flat output dynamics Linares-Flores et al. (2023),

$$\dot{y}_2 = \eta_2 + \lambda_1 (z_1 - y_2) \quad (34)$$

$$\dot{\eta}_2 = \lambda_0 (z_1 - y_2) \quad (35)$$

where,  $y_2 = \hat{z}_1$ ,  $z_1 = \left(\frac{1}{2}\right) (L_2 i_{L_2}^2 + C_2 v_{C_2}^2)$ , and  $\eta_2 = \hat{a}_1$ .

Where,  $a_1 = E_2 i_{L_2} - \frac{v_{C_2}^2}{R_2} - v_{C_2} i_{p_2}$ . This last expression corresponds to the output power system. Thus, we have

$$\widehat{i}_{p_2} = \frac{E_2 i_{L_2} - \frac{v_{C_2}^2}{R_2} - \eta_2}{v_{C_2}}, \quad v_{C_2} \neq 0$$

The observation error dynamics is given by  $e_{obs} = z_1 - y_2$ ,

$$\ddot{e}_{obs} + \lambda_1 \dot{e}_{obs} + \lambda_0 e_{obs} = -\frac{d}{dt} a_1 \quad (36)$$

The selection of observer gains

$$\lambda_1 = 2\zeta\omega_n; \quad \lambda_0 = \omega_n^2 \quad (37)$$

$$\omega_n \geq \frac{1}{RC}, \quad \zeta = 0.707$$

with these gains the observation error  $e_{obs}$  converges asymptotically to near zero when  $t \rightarrow \infty$ , which produces that  $e_\eta = i_{p_2} - \widehat{i}_{p_2}$  is radially enclosure and converges asymptotically to near zero. The constant desired references of (33) are:

$$\bar{u}_2 = \frac{E_2}{V_{d_2}}, \quad \bar{i}_{L_2} = \frac{V_{d_2}^2}{R_2 E_2} + \frac{V_{d_2}}{E_2} \widehat{i}_{p_2}$$

Notice that the estimated variable of the output current,  $\widehat{i}_{p_2}$  of the DC interconnection node, is adapted to the inductor current desired reference of the boost converter to obtain equitable active power contribution and synchronization with the rest of the DC power modules in the microgrid system.

### 2.3 Modelling and ESO-PBC for the AC/DC Boost Rectifier

The average model of the mono-phase boost rectifier is obtained employing Fig. 1 (c), and this is given by

$$L_3 \frac{di_{L_3}}{dt} = -r_{L_3} i_{L_3} - v_{C_3} u_3 + E_3 \sin(\omega_n t) \quad (38)$$

$$C_3 \frac{dv_{C_3}}{dt} = i_{L_3} u_3 - \left(\frac{1}{R_3}\right) v_{C_3} - i_{p_3} \quad (39)$$

The passivity-based controller is calculated similarly to the controller of the before section for the rectifier (38)-(39), is given by

$$u_3 = \bar{u}_3 + \gamma_3 V_{d_3} (i_{L_3} - \bar{i}_{L_3}) - \gamma_3 \bar{i}_{L_3} (v_{C_3} - V_{d_3}) \quad (40)$$

The reduced extended state observer to estimate the demand current for the DC microgrid in the node is

$$\dot{y}_3 = \eta_3 + \lambda_1 (h_1 - y_3) \quad (41)$$

$$\dot{\eta}_3 = \lambda_0 (h_1 - y_3) \quad (42)$$

where,  $y_3 = \hat{h}_1$ ,  $h_1 = \left(\frac{1}{2}\right) (L_3 i_{L_3}^2 + C_3 v_{C_3}^2)$ , and  $\eta_3 = \hat{a}_2$ .

Where  $a_2 = i_{L_3} E_3 \sin(\omega_n t) - \frac{v_{C_3}^2}{R_3} - r_{L_3} i_{L_3} - v_{C_3} i_{p_3}$ , corresponding to the output power system. Thus, we have the following

$$\widehat{i}_{p_3} = \frac{i_{L_3} E_3 \sin(\omega_n t) - \frac{v_{C_3}^2}{R_3} - r_{L_3} i_{L_3} - \eta_3}{v_{C_3}}, \quad v_{C_3} \neq 0$$

The constant desired references of rectifier controller (40) are

$$\bar{u}_3 = \frac{E_3 \sin(\omega_n t) - r_{L_3} \bar{i}_{L_3}}{V_{d_3}}, \quad \bar{i}_{L_3} = A \sin(\omega_n t)$$

where

$$A = \frac{E_3}{2r_{L_3}} - \sqrt{\left(\frac{E_3}{2r_{L_3}}\right)^2 - \left(\frac{2V_{d_3}^2}{r_{L_3}}\right) \left(\frac{1}{R_3} + \widehat{i}_{p_3}\right)}$$

Notice that the estimated variable of the output current,  $\widehat{i}_{p_3}$  of the DC interconnection node is adapted to the inductor current desired reference of the mono-phase rectifier to obtain equitable active power contribution and synchronization with the rest of the DC power modules in the microgrid system. We omit the stability proof of the observer controller in a closed loop because it is similar to the previous section. So, the results obtained in this section are almost identical to those in the last section.

## 3. PSIM SIMULATION RESULTS

This section aims to present simulations of a microgrid circuit on PSIM. 3 shows the output voltage response in each microgrid module. On the other hand, Figure 3 shows the load current response. These results demonstrate that the controller maintains a similar voltage and current level in each interconnected module. This reflects the convergence towards the desired value of the modules. In this sense, Figure 3 describes the output power in each microgrid module. Finally, Figure 3 presents the total active power consumed during the PSIM simulation load.

## 4. CONCLUSIONS

A decentralized PCB designed for DC/DC and AC/DC generation power modules connected to a DC microgrid. We use DC-to-DC buck and boost topologies for two power-generating modules, and the third is a rectifier based on a boost-type topology. Implementing different topologies and using the ESO demonstrated that the

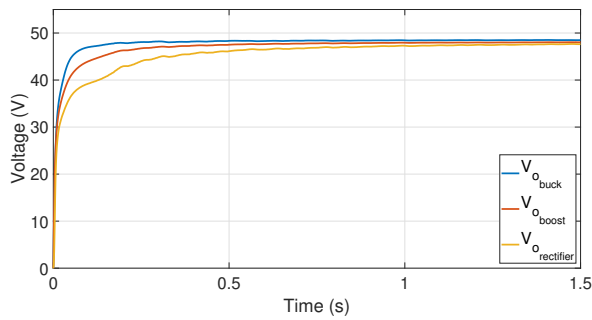


Fig. 2. Output voltage responses,  $v_{C_1}$ ,  $v_{C_2}$ , and  $v_{C_3}$ .

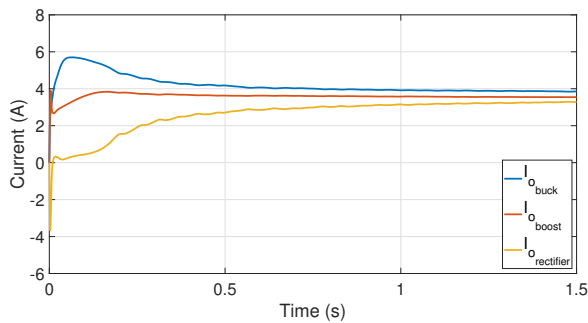


Fig. 3. Current responses in the power modules,  $i_{R_1}$ ,  $i_{R_2}$ , and  $i_{R_3}$ .

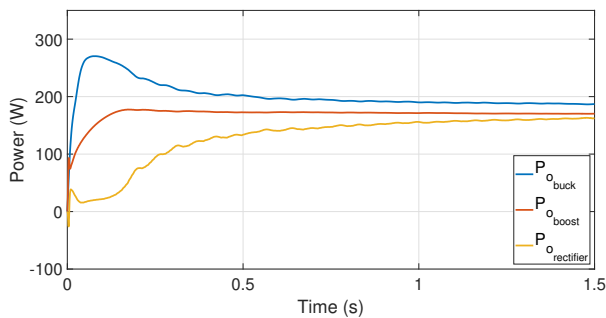


Fig. 4. Output power responses in each power module.

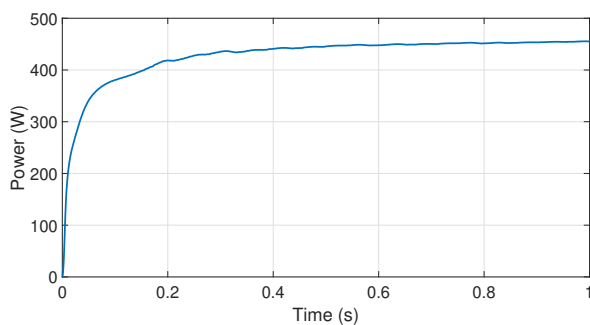


Fig. 5. Active power response at main load ( $z_L$ ).

passivity-based controllers achieve an equal contribution of power and synchronization at the microgrid's intercon-

nection node by adapting to the current demand. The PSIM simulation results showed the effectiveness and robustness necessary for the performance of the PCB controllers based on ESOs in closed-loop.

## REFERENCES

- Al-Ismail, F.S. (2021). Dc microgrid planning, operation, and control: A comprehensive review. *IEEE Access*, 9, 36154–36172. doi:10.1109/ACCESS.2021.3062840.
- Anand, S. and Fernandes, B.G. (2013). Reduced-order model and stability analysis of low-voltage dc microgrid. *IEEE Transactions on Industrial Electronics*, 60(11), 5040–5049. doi:10.1109/TIE.2012.2227902.
- Bai, W., Sechilariu, M., and Locment, F. (2020). Dc microgrid system modeling and simulation based on a specific algorithm for grid-connected and islanded modes with real-time demand-side management optimization. *Applied Sciences*, 10(7). doi:10.3390/app10072544.
- El-Shahat, A. and Sumaiya, S. (2019). Dc-microgrid system design, control, and analysis. *Electronics*, 8(2). doi:10.3390/electronics8020124.
- Espina, E., Llanos, J., Burgos-Mellado, C., Cárdenas-Dobson, R., Martínez-Gómez, M., and Sáez, D. (2020). Distributed control strategies for microgrids: An overview. *IEEE Access*, 8, 193412–193448. doi: 10.1109/ACCESS.2020.3032378.
- Feng, X., Liu, J., and Lee, F. (2002). Impedance specifications for stable dc distributed power systems. *IEEE Transactions on Power Electronics*, 17(2), 157–162. doi: 10.1109/63.988825.
- Linares-Flores, J., Hernández-Mendez, A., Juárez-Abad, J.A., Contreras-Ordaz, M.A., García-Rodríguez, C., and Guerrero-Castellanos, J.F. (2023). Mppt novel controller based on passivity for the pv solar panel-boost power converter combination. *IEEE Transactions on Industry Applications*, 59(5), 6436–6444. doi: 10.1109/TIA.2023.3274618.
- Liu, J., Feng, X., Lee, F., and Borojevich, D. (2003). Stability margin monitoring for dc distributed power systems via perturbation approaches. *IEEE Transactions on Power Electronics*, 18(6), 1254–1261. doi: 10.1109/TPEL.2003.818822.
- Loranca-Coutiño, J., Mayo-Maldonado, J.C., Escobar, G., Maupong, T.M., Valdez-Resendiz, J.E., and Rosas-Caro, J.C. (2022). Data-driven passivity-based control design for modular dc microgrids. *IEEE Transactions on Industrial Electronics*, 69(3), 2545–2556. doi: 10.1109/TIE.2021.3065615.
- Modu, B., Abdullah, M.P., Sanusi, M.A., and Hamza, M.F. (2023). Dc-based microgrid: Topologies, control schemes, and implementations. *Alexandria Engineering Journal*, 70, 61–92. doi: https://doi.org/10.1016/j.aej.2023.02.021.